The nucleotide-binding domain of the Zn^{2+}-transporting P-type ATPase from *Escherichia coli* carries a glycine motif that may be involved in binding of ATP

Juha OKKERI*, Liisa LAAKKONEN†[1] and Tuomas HALTIA*[1]

*Institute of Biomedical Sciences/Biochemistry, P.O. Box 63 (Biomedicum Helsinki, Haartmaninkatu 8), FIN-00014 University of Helsinki, Helsinki, Finland, and †Helsinki Bioenergetics Group, Structural Biology and Biophysics Programme, Institute of Biotechnology, P.O. Box 65 (Viikinkaari 1), FIN-00014 University of Helsinki, Helsinki, Finland

In P-type ATPases, the nucleotide-binding (N) domain is located in the middle of the sequence which folds into the phosphorylation (P) domain. The N domain of ZntA, a Zn^{2+}-translocating P-type ATPase from *Escherichia coli*, is approx. 13 % identical with the N domain of sarcoplasmic reticulum Ca^{2+}-ATPase. None of the Ca^{2+}-ATPase residues involved in binding of ATP are found in ZntA. However, the sequence G^{503}SGIEAQV in the N domain of ZntA resembles the motif GxGxxG, which forms part of the ATP-binding site in protein kinases. This motif is also found in Wilson disease protein where several disease mutations cluster in it. In the present work, we have made a set of disease mutation analogues, including the mutants G503S ($Gly^{503} \rightarrow$ Ser), G505R and A508F of ZntA. At low [ATP], these mutant ATPases are poorly phosphorylated. The phosphorylation defect of the mutants G503S and G505R can, however, be partially (G503S) or fully (G505R) compensated for by using a higher [ATP], suggesting that these mutations lower the affinity for ATP. In all three mutant ATPases, phosphorylation by P_i has become less sensitive to the presence of ATP, also consistent with the proposal that the Gly^{503} motif plays a role in ATP binding. In order to test this hypothesis, we have modelled the N domain of ZntA using the sarcoplasmic reticulum Ca^{2+}-ATPase structure as a template. In the model, the Gly^{503} motif, as well as the residues Glu^{470} and His^{475}, are located in the proximity of the ATP-binding site. In conclusion, the mutagenesis data and the molecular model are consistent with the idea that the two loops carrying the residues Glu^{470}, His^{475}, Gly^{503} and Gly^{505} play a role in ATP binding and activation.

Key words: copper, metal ion transport, nucleotide-binding domain, P_1-type ATPase, Wilson disease.

INTRODUCTION

A typical P-type ATPase uses the free energy of ATP hydrolysis to transport cations across a membrane. During the transport cycle, the enzyme becomes transiently phosphorylated at a conserved aspartyl residue. The most extensively characterized P-type ATPase is Ca^{2+}-ATPase isolated from rabbit sarcoplasmic reticulum. In addition to extensive mutagenesis and biochemical studies, its crystal structure has been determined in two different states (called E_1 and E_2) of the catalytic cycle. The structure of Ca^{2+}-ATPase in the E_1 state [1] shows that two Ca^{2+} ions are bound to the TM (transmembrane) domain which comprises ten TM helices. The large cytoplasmic portion of the ATPase comprises three well-separated structural entities: the actuator (A), phosphorylation (P) and nucleotide-binding (N) domains. To determine the second structure, the thapsigargin-inhibited protein was crystallized in the absence of Ca^{2+} ions. In this crystal structure, believed to represent the E_2 state, all three cytoplasmic domains are in contact with each other [2]. In comparison to the E_1 state structure, the largest changes include a rotation of the A domain by some 110° and a movement of the N domain, the top part of which shifts by as much as 50 Å. These changes are transmitted via the P domain to the TM part of the protein, so that structural alterations in the TM helices and the associated metal-binding site occur during the $E_1 \rightarrow E_2$ transition. Ion pumping is thought to result from the differential sidedness and affinity of the metal-binding site in the E_1 and E_2 states.

Despite the X-ray structures, several questions about the mechanism of catalysis remain unanswered. In particular, it is not understood how the ATP molecule, bound to a site in the N domain, donates its γ-phosphate to the active aspartate residue in the P domain (located some 20 Å from the nucleotide-binding site in both Ca^{2+}-ATPase structures). In Ca^{2+}- and Na^+,K^+-ATPases, the residues participating in nucleotide binding and in phosphoryl transfer (which also requires binding of a Mg^{2+} ion in the active site) have been studied by many groups [3–7]. In Ca^{2+}-ATPase, the residues Thr^{441}, Glu^{442}, Phe^{487}, Arg^{489}, Lys^{492}, Lys^{515}, Arg^{560} and Leu^{562} have been proposed to take part in ATP binding [4,5,8,9]. Recent experiments, in which ATP-Fe^{2+} was used to bring about side-chain oxidation or oxidative cleavage of the backbone in Ca^{2+}- and Na^+,K^+-ATPases, indicated that, in the E_1 state, the N domain residues K^{436}VGEA and the P domain residues N^{706}DAP are close to the bound ATP-Fe^{2+} (Ca^{2+}-ATPase sequence and numbering) [6,10]. In the E_2 state, the latter cleavage at residues 706–709 did not occur. Instead, cleavages were observed between residues Phe^{455}–Pro^{500} (where three of the residues affecting ATP binding are located, compare with above) in the N domain and also near the motif T^{181}GES in the A domain. The picture that emerges from these studies is that, in the N domain of Ca^{2+}-ATPase, residues in the segments Lys^{436}–Ala^{440} and Phe^{455}–Pro^{500} are close to the bound ATP-Mg^{2+} during the turnover of the enzyme. Other N domain regions which take part in ATP binding involve those with residues Lys^{515}, Arg^{560} and Leu^{562}. However, as shown in Figure 1, these residues are not conserved in ZntA

Abbreviations used: A domain, actuator domain; cAPK, cAMP-dependent protein kinase; N domain, nucleotide-binding domain; P domain, phosphorylation domain; PDB, Protein DataBank; TCA, trichloroacetic acid; TM, transmembrane; WD, Wilson disease; ZntA, Zn^{2+}-transporting P-type ATPase; G503S, $Gly^{503} \rightarrow$ Ser.

[1] To whom correspondence should be addressed (e-mail Haltia@cc.helsinki.fi or Liisa.Laakkonen@helsinki.fi).

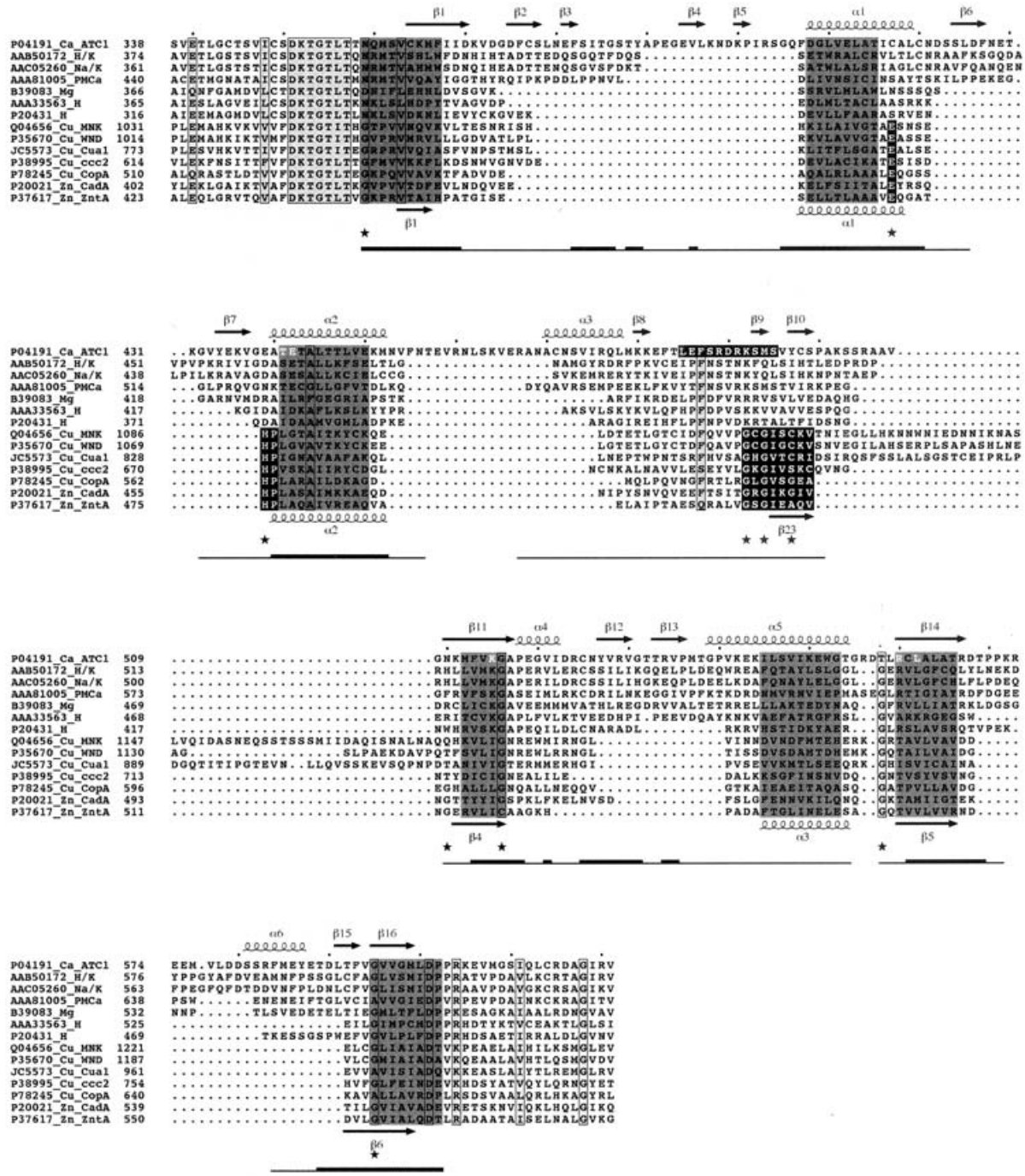

Figure 1 Alignment of N-domain sequences of P_1- and P_2-type ATPases

For heavy-metal-transporting ATPases, the term P_1-ATPases is used, whereas Ca^{2+}- and Na^+,K^+-ATPases are examples of non-heavy-metal-transporting or P_2-type ATPases (see [11,12]). The accession number of each sequence is on the left. The sequences are: P04191 (rabbit sarcoplasmic Ca^{2+}-ATPase), AAB50172 (human H^+,K^+-ATPase), AAC05260 (pig Na^+,K^+-ATPase), AAA81005 (rat plasma membrane Ca^{2+}-ATPase), B39083 (*Salmonella typhimurium* Mg^{2+}-ATPase), AAA33563 (*Neurospora crassa* H^+-ATPase), P20431 (*Arabidopsis thaliana* H^+-ATPase), Q04656 (Menkes disease protein, human Cu^+-ATPase), P35670 (WD protein, human Cu^+-ATPase), JC5573 (*Caenorhabditis elegans* Cu^+-ATPase), P38995 (*Saccharomyces cerevisiae* Cu^+-ATPase), P78245 (*E. coli* Cu^+-ATPase), P20021(*Staphylococcus aureus* Zn^{2+}-ATPase), P37617 (ZntA, *E. coli* Zn^{2+}-ATPase). Secondary structure of the rabbit sarcoplasmic Ca^{2+}-ATPase, based on the crystal structure 1IWO [2], is indicated with arrows and helix symbols above the sequences. Amino acid residues proposed to interact with ATP in Ca^{2+}-ATPase [4] are shown in white. Also other residues in the loop carrying Phe^{487}, Arg^{489} and Lys^{492} which are known to reside near the bound ATP, are shown in white with black background. The predicted secondary structure of ZntA is shown beneath the sequences. The bottom line indicates the magnitude of the temperature factor for each amino acid residue in the Ca^{2+}-ATPase crystal structure 1EUL [1]: thick line, $B < 35$ Å^2; thin line, 35 Å^2 < $B < 55$ Å^2; no line, $B > 55$ Å^2. Segments forming the core secondary structure elements are highlighted with dark grey. Well-conserved residues are boxed with a light grey background. The asterisks below the alignment indicate the ZntA residues mutated in the present study. In the P_1-ATPase sequences, black boxes are used to highlight the conserved residues Glu^{470} and His^{475}-Pro (ZntA numbering) and the Gly^{503} loop. The secondary structure prediction yielded only one β-strand (β23) near Gly^{503} of ZntA. However, a similar prediction was obtained for the glycine loop of cAPK, which, however, in reality is known to comprise two short antiparallel β-strands (a β-hairpin) [29]. Accordingly, in Figure 6, we have modelled the sequence G^{503}SGIEAQV using the structure of the glycine loop G^{50}TGSFGRV of the protein kinase as a template. Note that the Menkes (MNK), WD (WND) and *C. elegans* Cua1 protein contain an insertion of 35–50 residues between β23 and β4. One loop and a pair of β-strands with low temperature factors in the crystal structure of Ca^{2+}-ATPase, Phe^{382}–Tyr^{389} and Cys^{525}-Val^{535}, are not conserved in P_1-ATPases. However, inspection of the Ca^{2+}-ATPase structure reveals that they are located at the surface of the N domain (and not in the structural core of the protein).

(Zn^{2+}-transporting P-type ATPase) or in any other heavy-metal-transporting ATPase. The question therefore arises: how does ZntA bind ATP?

The alignment in Figure 1 combines information from analysis of sequence conservation, the crystal structures of Ca^{2+}-ATPase and secondary structure prediction of ZntA. Inspection of the alignment suggests that Ca^{2+}-ATPase residues 436–440 are structurally equivalent with the sequence around His^{475}-Pro of ZntA. The counterpart of Lys^{492} and its neighbours in Ca^{2+}-ATPase appears to comprise the sequence G^{503}SGIEAQV^{510} in ZntA. The His^{475}-Pro motif, as well as the Gly^{503} segment, are highly conserved in P_1-type ATPases. In addition, mutations of the equivalents of His^{475}, Gly^{503} and Gly^{505} in a human copper-ATPase cause Wilson disease (WD; reviewed in [13]), showing that these residues perform important structural and/or functional roles in heavy-metal-transporting ATPases.

In the present work, we have focused on the N domain of the Zn^{2+}-transporting P-type ATPase ZntA, which is a bacterial homologue of human Cu^{2+}-ATPases [14,15]. In our previous studies, we constructed several WD mutation analogues of ZntA, e.g., ZntA mutants E470A ($Glu^{470} \rightarrow Ala$) and H475Q, and characterized the mutant ATPases [16,17]. We concentrate in the present study on the Gly^{503} and His^{475}-Pro motifs in the N domain of ZntA. Furthermore, we have used the crystal structure of Ca^{2+}-ATPase, together with the alignment in Figure 1, to build a three-dimensional model of the N domain of ZntA. The model allows us to discuss the mutational effects in a structural context. Our results suggested that the segment G^{503}SGIEAQV^{510} is involved in binding of ATP, perhaps forming a glycine loop similar to that in the ATP-binding site of the cAPK (cAMP-dependent protein kinase) [18,19]. Amino acid residues Glu^{470} and His^{475} may also be part of the ATP-binding site. A part of this work has appeared in a preliminary form [20].

EXPERIMENTAL

Sequence alignment

The alignment in Figure 1 was constructed using ClustalX [21]. In order to create gap penalties for the program, the known secondary structure of sarcoplasmic Ca^{2+}-ATPase and the predicted secondary structure of ZntA (see below) were used. P-type ATPase sequences with the following PDB (Protein DataBank) accession codes were used as an input for ClustalX: sarcoplasmic reticulum Ca^{2+}-ATPases, P04191, S27763, O23087, Q9XES1, CAB96170, O43108, T40199, T20277, E69000 and BAB06234; plasma membrane Ca^{2+}-ATPases, AAA81005, CAB96189, CAA09308 and P28876; Na^+,K^+- and H^+,K^+-ATPases, AAF98360, AAC05260, AAB50172 and Q64392; H^+-ATPases, A64453, P20431, AAA33563 and CAA05841; Mg^{2+}-ATPases, P36640, AAG08210 and B39083; P_1-ATPases, P37617, Q9RZ81, P20021, P94888, Q59998, O26849, P32113, CAC07984, P78245, BAA96520, Q9SZC9, BAB04276, O69710, P05425, Q04656, P35670, JC5573, P38995 and P77871.

Secondary structure predictions

The secondary structure of ZntA was analysed using the PHD program (http://www.embl-heidelberg.de/predictprotein/) [22]. The input comprised all heavy-metal-ATPase sequences included in the list above. To test the reliability of the prediction program, the secondary structure of Ca^{2+}-ATPase was also analysed using the sequences of Na^+,K^+-ATPases and Ca^{2+}-ATPases in the above list (the plasma membrane Ca^{2+}-ATPases were not included) as the input. In general, the secondary structure prediction of Ca^{2+}-ATPase, carried out without information about the three-dimensional structure, agreed well with the secondary structure elements observed in the crystal structure. In particular, all the secondary structure elements (see Figure 1) which we propose to constitute the core of the N domain of P-type ATPases were predicted correctly when using only the Ca^{2+}- and Na^+,K^+-ATPase sequences as the input.

Modelling

The coordinates of sarcoplasmic Ca^{2+}-ATPase (PDB entry 1IWO), describing the Ca^{2+}-ATPase structure in the E_2 state at 3.1 Å resolution [2], were obtained from PDB. The correspondence between Ca^{2+}-ATPase and ZntA was established using secondary structure prediction and the sequence alignment (Figure 1). Sequence manipulations *in silico* and energy minimizations were carried out with the Homology and Discovery3 modules of Insight II (Accelrys). Energy minimizations consisted of 2000 steps and were done sequentially, first with side chains, then with loops and finally with the whole N-domain structure. Force field cff91 was used. The loop ranging from Gly^{503} to Val^{510} in ZntA has been positioned similarly with the Ca^{2+}-ATPase loop between residues Leu^{485} and Ser^{495}. This loop comprises residues Phe^{487}, Arg^{489} and Lys^{492}, suggested to interact with ATP in Ca^{2+}-ATPase (see, for example, [4]). The conformation of the segment G^{503}SGIEAQV of ZntA was then modelled using the structure of the glycine loop (G^{50}TGSFGRV) of cAPK (PDB entry 1ATP) as the template. The conformations of other loops connecting the conserved secondary structure elements were taken from PDB using Insight II loop search utility.

Mutagenesis

Mutants were generated using PCR and a ZntA construct as described previously [16,17]. Each mutation was verified by DNA sequencing.

Expression of His-tagged ZntA

Wild-type and mutated versions of ZntA were expressed as His-tagged recombinant proteins in *E. coli TOP 10* [17]. Expression of the protein was induced with 100 μM isopropyl β-D-thiogalactoside 1 h 45 min after inoculation. Cells were harvested 5 h after induction and stored at -20 °C.

Isolation of the membrane fraction and determination of the expression levels

Isolation of the membrane fraction from the cells was carried out as described previously [17]. The membranes were suspended into the storage buffer [50 mM Tris (pH 7.5)/300 mM NaCl/20 % glycerol/2 mM 2-mercaptoethanol/0.5 mM PMSF] to a final concentration of 10 mg of protein/ml and stored at -70 °C. Protein concentration was measured with the bicinchoninic acid protein assay kit (Pierce). The expression levels of the mutants were analysed using SDS/PAGE (10 % gels) combined with Coomassie Blue staining (30 μg of membrane protein per lane). Quantification of band intensities were done with ImageMaster VDS imaging system (Pharmacia Biotech) and AIDA software (version 2.00; Raytest Isotopenmessgeräte GmbH).

ATPase activity measurements

The Zn^{2+}-dependent ATPase activity of the membrane fraction was determined with the P_i analysis method in the absence or

presence of 20 μM $ZnSO_4$ [16]. ATP (4 mM) was used in the activity assay. The most active mutants (G444V, H475Q, G505R, G512W and C518P) were also characterized by measuring their activities at lower ATP concentrations (0.05–1.35 mM ATP). In these assays, an ATP-regenerating system, comprising 2 mM phosphoenolpyruvate and 5.4 units/ml pyruvate kinase, was used. The error bars in Figures 2, 4 and 5 show the S.D. for ten (Figure 2A), eight (Figure 2B) or four (Figures 4 and 5) independent measurements.

Phosphorylation assays

Phosphorylation of the ATPase by [γ-^{33}P]ATP and by [^{33}P]P_i (Amersham Pharmacia) was measured as described previously [17], except that the labelling time in P_i phosphorylation experiments was 12 min. In the experiments with different concentrations of ATP, the total concentrations of non-radioactive and radioactive ATP were as follows: total [ATP] = 60.3 nM ATP, comprising 58.0 nM ATP and 2.3 nM [γ-^{33}P]ATP; total [ATP] = 0.587 μM ATP, comprising 0.58 μM ATP and 6.9 nM [γ-^{33}P]ATP; total [ATP] = 5.82 μM ATP, comprising 5.80 μM ATP and 21.1 nM [γ-^{33}P]ATP; total [ATP] = 58.06 μM ATP, comprising 58.0 μM ATP and 61.5 nM [γ-^{33}P]ATP. The measured radioactivities were corrected for the different relative amount of labelled ATP in each reaction mixture with a different total [ATP].

The analysis of the phosphorylated samples on acidic SDS/PAGE (8 % gels) and imaging of the dried gels by a BAS-1800 Bio-imaging analyser (Fuji) were performed as described previously [17]. The phosphorylated bands are sensitive to hydroxylamine, with 250 mM hydroxylamine resulting in 50 % reduction in phosphorylation [23]. Only the analysis of the monomer (molecular mass approx. 92 kDa) and the dimer (molecular mass approx. 190 kDa) bands is included in the present study. The behaviour of 67 kDa band, which lacks the N-terminal metal-binding domain of ZntA [17], is qualitatively similar with the full-length protein, although its phosphorylation levels are generally lower, particularly in the mutants. The exposure times of the dried gels on the imaging plate were 6 h in ATP-titration experiments and 8 h in P_i-phosphorylation experiments.

Dephosphorylation assays

The measurement of dephosphorylation kinetics has been described previously [17]. The exposure times in dephosphorylation experiments varied from 6–24 h, depending on the phosphorylation level of the mutant. The results shown are independent of the exposure time.

RESULTS

Expression levels and activity

We report in the present work the characterization of the ZntA mutants G444V^{WD}, G503S^{WD}, G503D, G505R^{WD}, G505E, A508F^{WD}, G512W, C518P, G539R^{WD} and G553P. The mutations marked with the superscript 'WD' mimic Wilson disease mutations. Our main target has been to mutate glycine residues in the N domain of ZntA (Figure 1). Furthermore, in order to provide further insight into the role His^{475}, we have made several new substitutions of this residue. Two previously published mutants [16,17], H475Q^{WD} and E470A^{WD}, have been characterized further. The mutants and their properties are summarized in Table 1. SDS/PAGE and the measurement of Zn^{2+}-dependent ATPase activity of the bacterial membrane fraction were routinely used to evaluate the expression level and activity of each mutant. The levels of ZntA protein vary from no expression (G553P) or slight under-expression (G512W and C518P) to moderate over-expression (E470A^{WD}, H475D, H475S, G503S^{WD}, G503D and G505E). Mutations G444V^{WD}, H475A, H475L, H475Q^{WD}, G505R^{WD}, A508F^{WD} and G539R^{WD} result in expression similar to the wild-type. To take the different expression levels into account, the results of the activity and phosphorylation assays have been normalized so that the values reported do not depend on the amount of the ZntA protein. The highest Zn^{2+}-dependent ATPase activitites (100 %, 88 % and 60 % of wild-type activity) were measured with the mutants G512W, C518P and G505R^{WD} respectively (Figure 2A). The lowest activities (1–5 % of the wild-type level) were observed with the mutants H475D and H475L. Interestingly, the latter activities are significantly lower than that of the WD mutant analogue H475Q^{WD} (whose activity is 43 % of the control [16,17]). The rest of the mutants have 8–32 % of wild-type ATPase activity.

In the above assay, 4 mM ATP was used. Although close to the physiological concentration, it is approx. 100-times the ATP concentration required for the half-maximal activity of wild-type ZntA (Figure 2B). Thus the fairly high activities of some mutants [G444V^{WD}, H475Q^{WD}, G505R^{WD}, G512W and C518P; 32–100 % of the wt (wild-type) activity] might reflect the relatively high [ATP] used. For this reason, we decided to extend the analysis to lower concentrations of ATP with these active mutants. The results in Figure 2(B) show that also these mutants have much lower ATPase activities when [ATP] is below 0.45 mM. We concluded that all our mutants have very clear functional defects.

Phosphorylation by [γ-^{33}P]ATP in different concentrations of ATP

A characteristic feature of P-type ATPases is that they catalyse the transfer of the γ-phosphate of ATP to a conserved aspartate side chain (Asp^{436} in ZntA [24]) as a part of the mechanism in which the energy of ATP is used to drive ion translocation. The formation of the aspartyl phosphate in the presence of the substrate ion and ATP can be monitored using [γ-^{33}P]ATP. We have quantified the phoshorylation levels of the mutant ATPases with ATP concentrations in the range 60 nM–58 μM (Figure 3). With a submicromolar [ATP], all the mutants targeted to Glu^{470}, His^{475}, Gly^{503} and Ala^{508}, as well as the substitution G505E, show less than 14 % of the wild-type phosphorylation level. The mutant G505R^{WD} shows a mild phenotype (50 % of the wild-type phosphorylation at 60 nM ATP), whereas phosphorylation of the G539R^{WD} ATPase systematically exceeds the wild-type level. At 58 μM ATP, the mutant proteins E470A^{WD}, A508F^{WD} and G505E remain poorly phosphorylated, yet the relative enhancement in the phosphorylation of the G505E ATPase is moderately strong (from 0.1 % at 60 nM ATP to 19 % at 58 μM ATP). It is, however, of note that, upon increasing [ATP], the phosphorylation levels of the mutants H475Q^{WD}, G503D, G503S^{WD}, G505R^{WD} and C518P increase rather steeply, almost reaching or even exceeding the wild-type level. In contrast, the phosphorylation of the mutants G444V^{WD} and G512W show less pronounced dependence on [ATP]. Taken together, the above results showed that the phosphorylation defect caused by mutations at Gly^{503} and Gly^{505}, as well as H475Q^{WD}, can be at least partially compensated for by increasing [ATP]. Consequently, these residues seem to influence the enzyme's apparent affinity for ATP.

Phosphorylation by [^{33}P]P_i in the presence of ATP or Zn^{2+}

The active aspartate of P-type ATPases can also be phosphorylated by P_i. This reaction is thought to occur when the enzyme is in the E_2 state, so that the product of the reaction can be denoted E_2-P

Table 1 Summary of the properties of the mutants

WD mutation analogues are underlined (Column 1). Expression levels (Column 2) were estimated from the intensity of SDS/PAGE bands using four different membrane preparations as described in the Experimental section. ATPase activities relative to the wild-type at 4 mM and 0.45 mM ATP are shown in Columns 3 and 4. The phosphorylation levels with 60 nM and 58 μM ATP are indicated in Columns 5 and 6. The next three Columns show phosphorylation levels with P_i (Column 7), with P_i in the presence of 1 mM ATP (Column 8) and with P_i in the presence of 100 μM Zn^{2+} (Column 9). The dephosphorylation rates of selected mutants (relative to the wild-type) in the presence or absence of ADP are indicated in Columns 10 and 11. Column 12 shows our conclusions about the behaviour of each mutant.

		ATPase activity (%)		[^{33}P]ATP (%)		[^{33}P]P_i (%)			Dephosphorylation rate		
Mutant	Expression (%)	4 mM ATP	0.45 mM ATP	60 nM ATP	58 μM ATP	–	1 mM ATP	100 μM Zn^{2+}	– ADP	+ ADP	Conclusions
1	2	3	4	5	6	7	8	9	10	11	12
Wild-type	100	100	79	14	100	100	12	16	Normal	Normal	
G444V	92	32	0.9	2.6	43	305	83	17			Stabilizes the E_2-P state; Gly^{444} might become close to P upon domain movements
E470A	184	17		0.1	5.2	86	79	17			Likely to play a role in ATP-binding site, located at the bottom of the ATP-binding cleft
H475A	115	8		0.3	34	44	8	6	Very low*	Very low*	Reacts poorly with ATP, influences the binding of ATP and also other catalytic steps
H475D	168	1		0.1	6.6	11	5	4			As above
H475L	110	5		0.6	24	15	4	6			As above
H475S	139	16		0.1	10	43	14	11			As above
H475Q	106	43	6	0.3	62	29	6	6	Very low†	Very low†	WD analogue, similar, but milder, phenotype than with the other substitutions above
G503S	133	22		0.7	57	161	78	36	low	Very low	Influences ATP-binding and stabilizes E_2-P
G503D	136	22		1.9	73	83	26	6			Influences ATP-binding site
G505E	159	11		0.1	19	85	41	11			As above, but stronger effect
G505R	90	60	13	7.1	121	88	23	14	Normal	Low	As above, but milder effect
A508F	116	11		0.1	5.6	30	18	8			Influences ATP-binding site and affects the E_2 conformation
G512W	64	100	21	3.6	58	95	14	19			Influences ATP-binding site and structural stability
C518P	54	88	12	1.2	67	65	32	12			Influences ATP-binding site and structural stability
G539R	113	12		24	117	7	1	3			Favours the E_1 state
G553P	–	–	–	–	–	–	–	–			Not expressed, plays a structural role in the N domain core

* The H475A ATPase is poorly phosphorylated by ATP. For this reason, it had to be phosphorylated using a higher [ATP], which results in a different [ADP]/[ATP] compared with the other mutants during the dephosphorylation phase. The mutant protein dephosphorylates in the presence and absence of added ADP at a lower rate than the wild-type ATPase, but owing to the difference in [ADP]/[ATP], the rate cannot be directly compared with the dephosphorylation rates of the other mutants.

† The rates have been measured in [17].

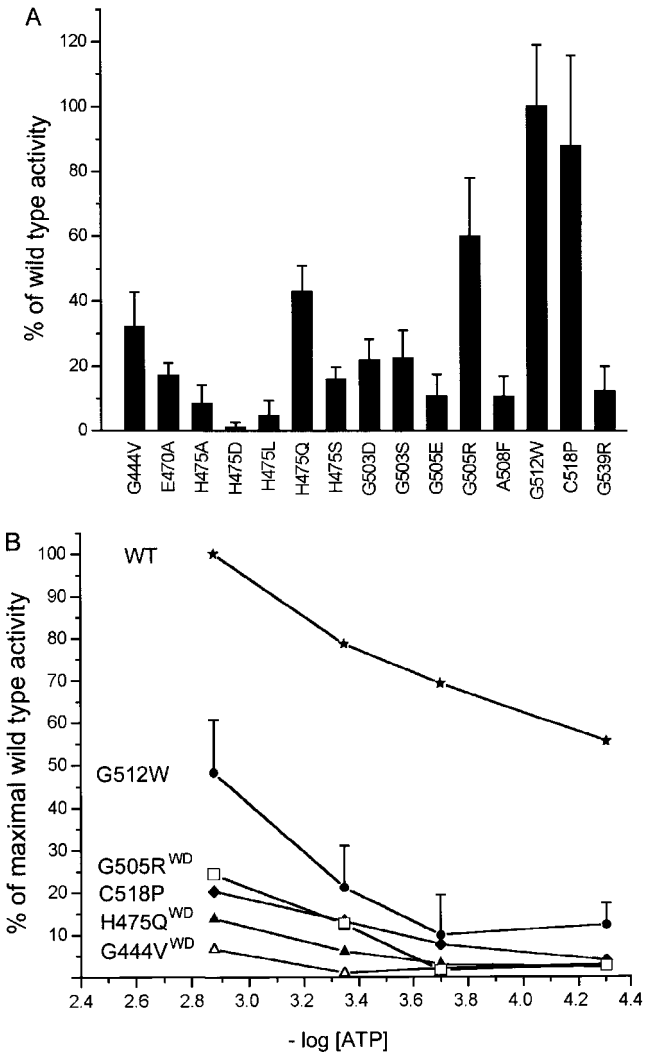

Figure 2 Zn^{2+}-dependent ATPase activities of the wild-type and mutant membranes (A) and Zn^{2+}-dependent ATPase activities of selected mutants in different ATP concentrations (B)

(**A**) Of the mutants mimicking WD mutations, the $G505R^{WD}$ ATPase has the highest activity and $G539R^{WD}$ the lowest. The mutant $H475Q^{WD}$ has 40 % of the wild-type activity, but all other substitutions of His^{475} result in much lower activities. The concentrations of Zn^{2+} and ATP were 20 μM and 4 mM respectively. The results are expressed as the means ± S.D. for 10 independent measurements. (**B**) The activities of mutants with more than 30 % of the wild-type (WT) activity at 4 mM ATP [see (**A**)] were measured as a function of ATP concentration in the range 0.05–1.35 mM. The results are expressed as the means ± S.D. for 8 independent measurements.

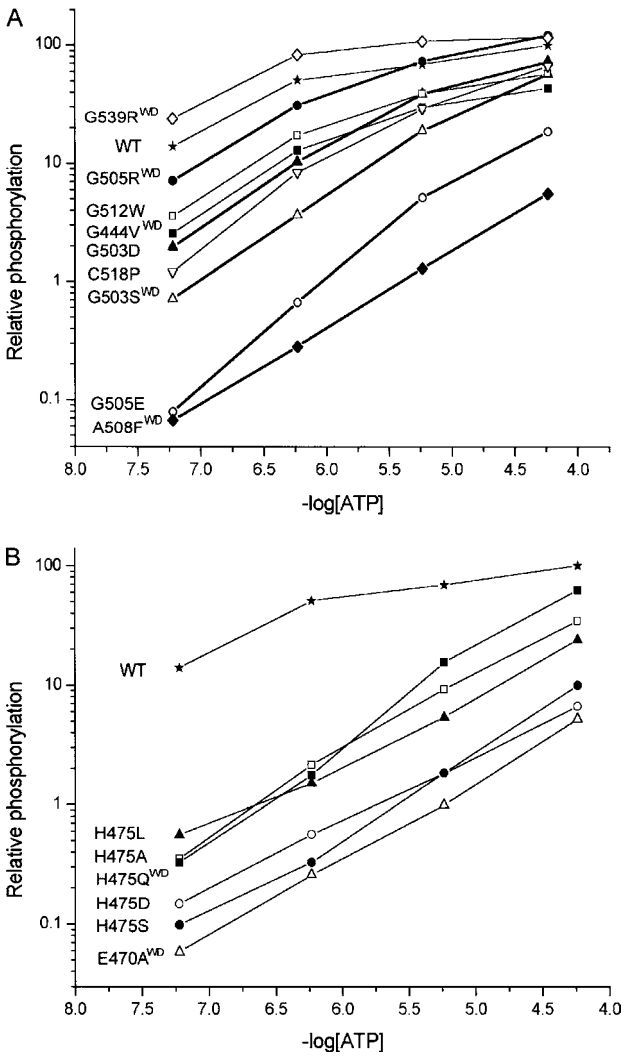

Figure 3 Phosphorylation of ZntA, with substitutions at Gly^{444}, Gly^{503}, Gly^{505}, Ala^{508}, Gly^{512}, Cys^{518} and Gly^{539}, by [γ-^{33}P]ATP as a function of ATP concentration (A) and phosphorylation of the H475 and $E470A^{WD}$ mutants (B)

(**A**) The curves for the mutants of the Gly^{503} motif are in **bold**. It is of note that the slopes of the curves of the $G503S^{WD}$ and G505E ATPases are relatively steep, contrary to the behaviour of the wild-type (WT) and the mutants $G444V^{WD}$, G512W and $G539R^{WD}$. (**B**) The steepest slope is observed with the $H475Q^{WD}$ ATPase.

(as opposed to the immediate product of the reaction with ATP, which is E_1-P). The formation of the E_2-P intermediate thus reflects the capability of the enzyme to adopt the E_2 state. ATP binds to E_1 with a submicromolar affinity constant, whereas in E_2 the affinity constant is some thousand-fold higher [25–28]. Consequently, a millimolar [ATP] stabilizes the enzyme in E_1 so that P_i should not phosphorylate it efficiently, provided that the ATP-binding site is intact.

The behaviour of the mutants in the P_i-phosphorylation experiment (Figure 4) can be divided into four categories. The first group includes the mutants $G444V^{WD}$ and $G503S^{WD}$. Their phosphorylation by P_i is clearly enhanced compared with the wild type. Furthermore, their E_2-P state is relatively resistant to the presence of ATP. This behaviour suggests that they tend to occupy the E_2 state and that ATP cannot convert them efficiently to the E_1 state. The second group (mutants which change His^{475}, and $G539R^{WD}$) phosphorylates more weakly than the wild-type. Members of the third category ($A508F^{WD}$ and C518P) are also hypophosphorylated, but unlike the previous group, their E_2-P state is partially resistant towards ATP. Finally, whereas P_i reacts with the $E470A^{WD}$, G503D, $G505R^{WD}$ and G505E ATPases similar to the wild-type ZntA, their E_2-P is clearly less sensitive to the presence of ATP than is the case with the wild-type. The G512W mutant resembles the wild-type in its P_i-phosphorylation properties.

Binding of the substrate Zn^{2+} to its binding site (thought to comprise the cysteines in the motif Cys^{392}Pro-Cys in the TM domain) takes place in the E_1 state. Because P_i can react only in the E_2 state, wild-type ZntA phosphorylation by P_i does not occur efficiently in the presence of Zn^{2+}. In other words, measuring the Zn^{2+} sensitivity of E_2-P is another way to study the conformational $E_2 \rightarrow E_1$ transition of the mutants. Comparison of the Zn^{2+} and ATP sensitivities of the E_2-P states of the mutants allows us to

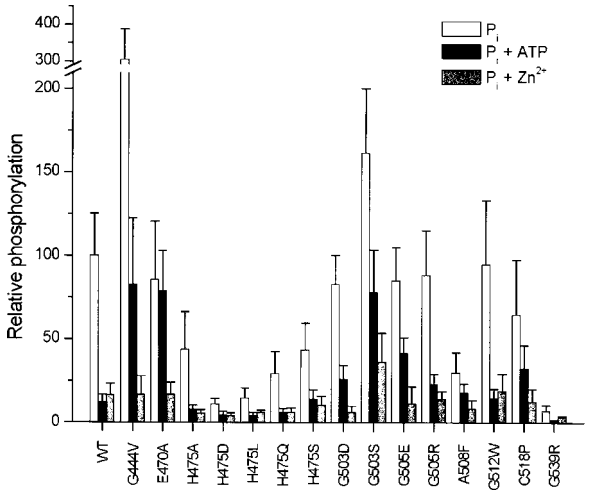

Figure 4 Phosphorylation of wild-type (WT) and mutant ATPases by [^{33}P]P_i in the absence and presence of 1 mM ATP or 100 μM Zn^{2+}

The results are expressed as the means ± S.D. for 4 independent measurements. The G444V^{WD} and G503S^{WD} ATPases are hyperphosphorylated, whereas the mutants at His^{475}, A508F^{WD} and G539R^{WD} are hypophosphorylated. Phosphorylation of the former group, as well as that of the relatively normal phosphorylated mutants E470A^{WD} and G505E, is relatively resistant toward the presence of 1 mM ATP. The E_2-P of the G503S^{WD} ATPase partially persists at 100 μM Zn^{2+}. Regarding the behaviour of His^{475} substituents, phosphorylation of the uncharged His^{475} mutants seem to be related to the size of the substituent, so that a smaller side chain results in a higher phosphorylation level.

differentiate between mutational effects on the conformational transition and effects on binding of ATP. In spite of the presence of 100 μM Zn^{2+}, the G503S^{WD} ATPase is phosphorylated much more intensely than the wild-type (Figure 4), although its phosphorylation level in the presence of Zn^{2+} is lower than in the presence of ATP (Table 1). It appears as if this mutant ATPase has a preference for occupying the E_2 state, or that in this mutant the metal-binding and phosphorylation sites do not communicate as in the wild-type enzyme. The E_2-P state of the mutants G444V^{WD}, E470A^{WD}, G503D, G505R^{WD} and G505E was sensitive to Zn^{2+}, but exhibits at least moderate resistance toward ATP. We conclude that the latter mutations interfere with binding of ATP, although the mutations G444V^{WD} and G503S^{WD} appear to cause an additional stabilization of the E_2-P conformation.

Dephosphorylation kinetics

The aspartyl phosphate of a P-type ATPase can decay via two routes: along the normal forward-reaction path, or, if extra ADP is present, via a reverse path with concomitant generation of ATP (see [17]). If a mutation, such as those discussed above in the G^{503} motif, influences nucleotide binding, the ADP-dependent dephosphorylation rate of the mutant ATPase is expected to decrease. Taking this into consideration, we have studied the dephosphorylation kinetics of the G503S^{WD} and G505R^{WD} ATPases (Figure 5).

The ADP-dependent dephosphorylation rate of the G503S^{WD} ATPase is clearly lower (Figure 5A). The G505R^{WD} protein also reacts with ADP at a significantly lower rate than the wild-type. In the forward reaction, i.e. without added ADP, the G503S^{WD} ATPase dephosphorylates slightly slower than the wild-type, whereas the G505R^{WD} protein behaves almost like the wild-type ATPase (Figure 5B). The dephosphorylation experiment is thus consistent with the idea that the residues Gly^{503} and Gly^{505} are involved in nucleotide binding. However, although the

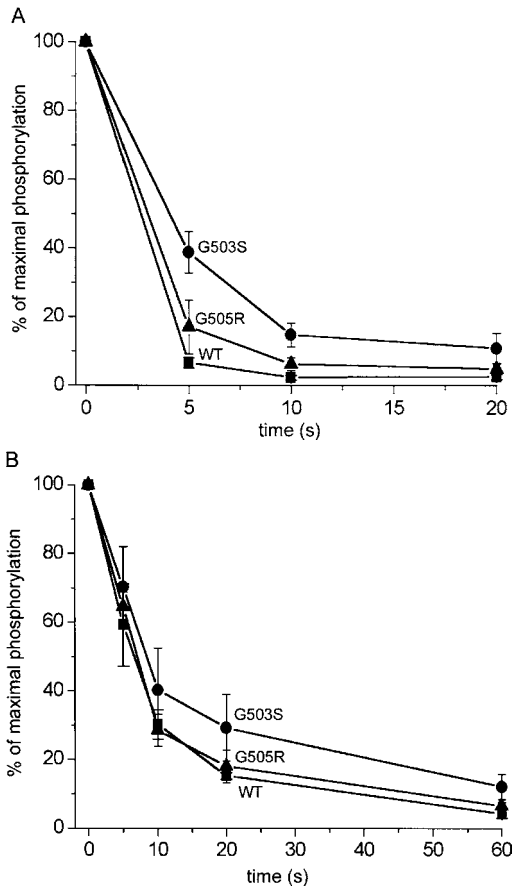

Figure 5 Dephosphorylation kinetics in the presence and in the absence of ADP

(**A**) The ADP-dependent dephosphorylation rates of the wild-type (WT), G503S^{WD} and G505R^{WD} proteins. Note the slow dephosphorylation rate of the G503S^{WD} ATPase. Membrane samples were phosphorylated with [γ-^{33}P]ATP for 30 s as described in the Experimental section. The reaction was then stopped with 250 μM ADP and 5 mM EDTA, and samples were collected at time points indicated. The level of phosphorylation was determined by applying 25 μg of membrane protein on a lane of an acidic SDS/PAGE gel followed by quantification of the radioactivity of the dried gel. (**B**) The rate of dephosphorylation in the absence of ADP. The reaction was stopped with 5 mM EDTA. Other conditions are as in (**A**).

G503S^{WD} ATPase reacts poorly with ADP, its slightly decreased ADP-independent dephosphorylation rate indicates an additional defect in the catalytic cycle.

DISCUSSION

One of the key steps in the transport cycle of P-type ATPases involves binding of an ATP molecule to the N domain of the ATPase, followed by the transfer of the γ-phosphate of the bound ATP to the active aspartate in the P domain. Although the molecular mechanism of the interdomain phosphoryl transfer remains to be established, a detailed picture of the nucleotide-binding site in Ca^{2+}-ATPase is emerging (see, for example, references [1,4]). In contrast, the situation with ZntA is much more unclear: all the amino acid residues constituting the ATP-binding site of Ca^{2+}-ATPase are missing from ZntA (Figure 1). Yet, there is a striking similarity between the predicted and observed secondary structure elements of ZntA (or WD protein) and Ca^{2+}-ATPase respectively. In addition, a number of WD mutations occur in the regions which correspond to those forming the ATP-binding

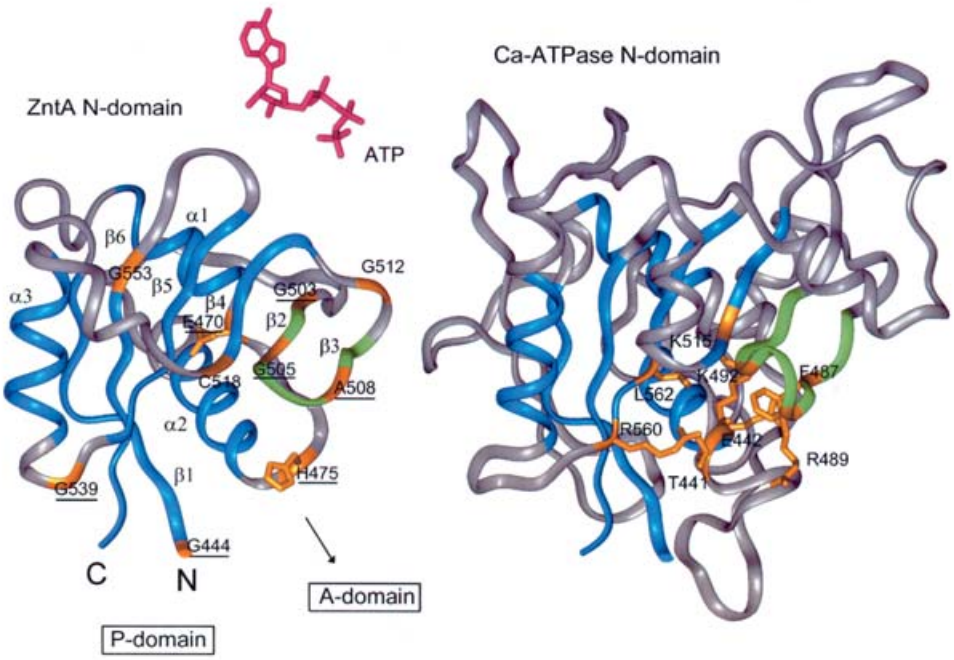

Figure 6 Molecular model of the N domain of ZntA based on the crystal structure of Ca^{2+}-ATPase (PDB entry 1IWO) [2], secondary structure predictions and sequence analysis of ZntA and other P-type ATPases (see Figure 1)

The structure of the template is shown in the right-hand panel. Note the larger size of the Ca^{2+}-ATPase N domain brought about by insertions of several β-sheets and two α-helices between the conserved elements. In the three-dimensional structure, these insertions are located on the surface of core structure. The blue colour indicates the areas constituting the conserved core of the domain. The amino acid residues we have mutated in the present work are shown in orange, which is also used to indicate the residues involved in ATP binding in Ca^{2+}-ATPase. WD mutation analogues are underlined. The Gly^{503} loop in ZntA, modelled using the glycine loop of cAPK as a template, and the Ca^{2+}-ATPase loop carrying three ATP-binding residues (Phe^{487}, Arg^{489} and Lys^{492}) are displayed in green. An ATP molecule (pink), taken from the crystal structure of cAPK (PDB entry 1ATP), is shown to provide a molecular scale. The approximate locations of the P and A domains are indicated.

site in Ca^{2+}-ATPase. Do these WD mutations interfere with ATP binding? In order to address this question, we have made 14 different amino acid substitutions in ZntA, the main theme being the role of glycine residues in the N domain of the enzyme. Five of the newly developed mutants ($G444V^{WD}$, $G503S^{WD}$, $G505R^{WD}$, $A508F^{WD}$ and $G539R^{WD}$) mimic WD mutations (note that, in the WD protein, the counterpart of Ala^{508} is Cys^{1104}). The properties of the mutants are summarized in Table 1. Briefly, our results suggest that the motifs G^{503}SGIEAQV^{510} and His^{475}-Pro, as well as the residue Glu^{470}, participate in nucleotide binding in the N domain of ZntA. Notwithstanding the low degree of identity between the N domains of Ca^{2+}-ATPase and ZntA, we have, after a careful sequence analysis, found a way to build a molecular model of the ZntA N domain using the Ca^{2+}-ATPase structure as a template. Although hypothetical, the model provides us with a structural framework for analysis of the mutagenesis data (Figure 6, and see below).

The molecular model of the N domain of ZntA

The N domain of Ca^{2+}-ATPase comprises the residues Asn^{359}–Pro^{602} [1]. In ZntA, the domain is significantly smaller, ranging from Gly^{444}–Thr^{560} (Figure 1). The identity between the sequences is about 13 %, posing a challenge for the modeller to use the Ca^{2+}-ATPase structure as a template for the ZntA N domain. However, secondary structure predictions imply that the order and type of secondary structure elements in both ATPases are similar. Superimposing the Ca^{2+}-ATPase structure and the secondary structure prediction for ZntA with the sequence alignment (Figure 1) suggests that the N domains of both ATPase subclasses share a similar core structure.

As mentioned above, ZntA lacks the amino acid residues proposed to be involved in binding of ATP in Ca^{2+}-ATPase. The differences occur mainly in two regions: firstly, a loop between helices $\alpha1$ and $\alpha2$, containing two short β-strands in Ca^{2+}-ATPase, has been replaced by a turn comprising the sequence VE^{470}QGATH^{475}P. Glu^{470} is thus located at the end of helix $\alpha1$, whereas the His^{475}-Pro motif, typical for heavy metal ATPases [29,30], resides at the beginning of helix $\alpha2$. Secondly, the region between helix $\alpha3$ and strand $\beta11$ of Ca^{2+}-ATPase, carrying the ATP-contacting residues Phe^{487}, Arg^{489} and Lys^{492}, contains three short strands ($\beta8$, $\beta9$ and $\beta10$) in a loop structure (shown in green in Figure 6). In ZntA, this part has been partially replaced with the sequence G^{503}SGIEAQV^{510}, predicted to form only one strand (strand $\beta23$ in Figure 1). However, the ATP-binding loop of cAPK (G^{50}TGSFGRV) was also predicted to form only one strand, although the crystal structure shows it to comprise two short antiparallel β-strands [31]. Accordingly, we have modelled the fold of the sequence G^{503}SGIEAQV using the structure of cAPK (PDB entry 1ATP) as a template. The loop has been positioned analogously with the Phe^{487} and Lys^{492} containing loop of Ca^{2+}-ATPase, but the direction of the backbone of the green loops is the opposite (see Figure 6). Modelling was done in this way to allow the Gly^{503} loop to interact with ATP, similarly to the template loop in cAPK, but other modes of interaction and, consequently, another direction of the backbone is possible.

The model can be used to analyse the three-dimensional locations of WD mutations, which occur in some 28 positions in the N domain [WD mutation database available from http://www.uofa-medical-genetics.org/wilson/index.php]. The majority of these (20) cluster into the right half of the N domain when strand β5 is used to divide the model into two parts, implying that this part of the domain is central to the function of the ATPase.

The Gly^{503} motif and nucleotide binding

In a number of nucleotide-binding proteins, glycine-rich signature sequences seem to form the key parts of nucleotide-binding sites [18,33,34]. In protein kinases, such as cAPK, the motif GxGxxG with three highly conserved glycines is found as a part of a β-hairpin structure which interacts with ATP [31]. While the exact way of binding of ATP even to Ca^{2+}-ATPase is not known, the similarity of the G^{503} motif of ZntA to the protein kinase glycine motif is interesting. This resemblance, together with the occurrence of several disease mutations in the equivalent motif of WD protein, prompted us to study the role of the Gly^{503} motif of ZntA.

Changing of either of the glycines or the alanine in the Gly^{503} motif (Figure 1) results in mutant ATPases with 11–60% of the wild-type activity. Particularly, the substitution $G503S^{WD}$ yields an ATPase that is poorly phosphorylated at low [ATP], but becomes more normal at a higher [ATP]. The finding that poor phosphorylation by ATP can be compensated for by increasing the concentration of ATP might be an indication of a change at the ATP-binding site. Furthermore, unlike the wild-type and His^{475} mutants, the P_i phosphorylation of Gly^{503} and Gly^{505} mutants is relatively resistant to the presence of ATP. As this phenomenon reflects binding of ATP to its binding site in the N domain with a concomitant stabilization of the E_1 state, this finding is also agreement with a mutation-induced change in the nucleotide-binding site. The third mutant of this predicted loop region, $A508F^{WD}$, has low activity and is weakly phosphorylated by both ATP and P_i. Yet its remaining P_i phosphorylation is relatively insensitive to the presence of ATP, an indication that Ala^{508} could also play a role in the binding site for ATP.

Other N-domain glycines

Of the three other glycine mutants ($G444V^{WD}$, G512W and $G539R^{WD}$), the first one shares many properties with the mutant $G503S^{WD}$. In particular, the $G444V^{WD}$ ATPase is hyperphosphorylated by P_i and its E_2-P appears somewhat resistant toward the presence of ATP (Table 1). We interpreted these findings as evidence for an abnormally stable E_2-P state. Inspection of the molecular model showed that Gly^{444} faces the P domain and could also be near the ATP-binding region when N and P domains interact during catalysis. The G512W ATPase has a reduced expression level and a defect in phosphorylation by ATP. It is fully active at 4 mM ATP (Figure 2A), but its activity is markedly impaired at lower ATP concentrations (Figure 2B). In the molecular model, G^{512} is predicted to be part of a turn leading to β-strand β4 and is located above the G^{503} loop (Figure 6). It might constitute a peripheral part of the nucleotide-binding site, but it could also influence the conformation of the G^{503} loop. The third mutant, $G539R^{WD}$, exhibits a combination of low ATPase activity, slight overphosphorylation by ATP and a striking hypophosphorylation by P_i. We interprete these properties as evidence for an abnormally stable E_1 state. Sequence analysis shows that Gly^{539} is almost fully conserved within P-type ATPases; in the model, it resides at a borderline between a turn and β-strand β5, and is located on the interface between N and P domains away from the nucleotide-binding region (Figure 6).

The mutation of C518P, although not substituting a glycine, targets a residue which is almost always a glycine residue (Figure 1). The model suggests that C^{518} is located near the nucleotide-binding site. This view is also consistent with properties of the mutant: compensation of low activity and phosphorylation by ATP by increasing [ATP] and reduced sensitivity of E_2-P to the presence of ATP.

The roles of Glu^{470} and His^{475}

Glu^{470} is very well conserved among P_1-ATPases and appears to be located deep on the bottom of the putative nucleotide-binding site in the model. The most conspicuous feature of the $E470A^{WD}$ ATPase is its highly ATP-resistant phosphorylation by P_i. We previously concluded that this mutant favours the E_2 state [16], based on the observed two-fold hyperphosphorylation by P_i. However, our present results show that there also tends to be about two-fold over-expression of the $E470A^{WD}$ mutant protein (Table 1). This higher amount of the mutant protein, which we did not observe previously, can account for the hyperphosphorylation phenotype. Our current view is that the $E470A^{WD}$ ATPase has a defect in ATP binding, which manifests itself as a relatively ATP-resistant E_2 state.

The sequence alignment (Figure 1) suggests that the His^{475}-Pro motif constitutes the beginning of helix α2, which lines the nucleotide-binding site (Figure 6, left-hand panel). In Ca^{2+}-and Na^+,K^+-ATPases the corresponding sequences are G^{438}EATE and V^{440}AGDA respectively. On the basis of ATP-Fe^{2+}-catalysed oxidative cleavage studies, Thr^{441} in the former and Asp^{443} in the latter have been proposed to participate in binding of Mg^{2+} [6,10]. In the present paper, we have characterized four new substitutions of His^{475}. All these mutants are expressed well, but their ATPase activities (1–16% of wild-type activity) are much lower than the activity of the previously published variant $H475Q^{WD}$ [16,17]. The hydrogen-bonding capability of the side chain may play a role in catalysis, because the $H475Q^{WD}$ and H475S mutants have clearly higher activities than the proteins with aliphatic substitutions H475A and H475L. The H475D ATPase is practically inactive, implying that a negative charge cannot be tolerated in this position. At a low [ATP], all the His^{475} mutants (including $H475Q^{WD}$) are very poorly phosphorylated. This defect is partially relieved at a higher [ATP] (Figure 3B and Table 1), the effect being clearest with the $H475Q^{WD}$ protein. In addition, the $H475Q^{WD}$ ATPase shows very slow ADP-dependent dephosphorylation [17]. Taken together, these data suggested that H^{475} is also among the residues which could contact the bound ATP. It should be noted, however, that the low rate of dephosphorylation along the forward-reaction path implies that there is also a more complex defect of catalysis in the $H475Q^{WD}$ protein (compare with reference [35], and see below).

All the His^{475} mutants have impaired P_i phosphorylation, which is also the case with WD protein mutated at the equivalent position [35]. The remaining phosphorylation is sensitive to ATP, which makes these mutants different from the mutants targeting the residues Gly^{444}, Glu^{470}, Gly^{503}, Gly^{505} and Ala^{508}, all of which cluster around the likely ATP-binding site in Figure 6. Interestingly, the level of P_i phosphorylation of the H^{475} mutants may to some extent correlate with the molecular volume of the substituting side chain, so that a larger volume brings about a more severe defect in phosphorylation by P_i. However, as in the activity measurements, the substitution H475D (i.e. substutition with a

small but negatively charged residue) yields the most severely affected protein, with 11% of the wild-type P_i phosphorylation remaining. In the model, the side chain of H^{475} is solvent exposed. The volume effect could therefore be due to an interaction with another domain of the ATPase (see below).

As noted already, His^{475} resides at the beginning of helix $\alpha 2$. The equivalent region of Ca^{2+}-ATPase is located on the N-domain surface which, in addition to carrying residues involved in Mg^{2+}-ATP binding, is thought to interact with the A domain during catalysis. The alignment in Figure 1 suggests that His^{475} is the equivalent of Glu^{439} of Ca^{2+}-ATPase. In the E_2 structure, Glu^{439} is within 3 Å of the A domain [2]. The latter is also known as the phosphatase domain, as it is implicated in the hydrolysis of the E_2-P intermediate of the catalytic cycle (see, for example, [36]). Consequently, the low dephosphorylation kinetics and the poor P_i-phosphorylation efficiency of the His^{475} mutants, dependent on the size of the substituting side chain, might reflect a perturbation in the interaction between the N and A domains, which is crucial in the catalysis of P-type ATPases [2,37–39]. Nevertheless, the observation that the poor phosphorylation at low [ATP] can be partially compensated for by elevating [ATP] implies a defect of ATP binding in the E_1 state. Assuming that both phosphorylation by ATP and the subsequent $E_1\text{-}P \rightarrow E_2\text{-}P$ transition are slow compared with the binding of ATP, the results in Figure 3(B) are consistent with about a 100-fold reduction in the affinity of the $H475Q^{WD}$ ATPase for ATP. This value is in line with the apparent $K_m{}^{ATP}$ values of 2000 μM and 16 μM, determined for the H1086Q mutant and the wild-type Menkes disease protein respectively [40]. A perturbation in nucleotide binding was also seen in the WD protein mutated at H^{1069}, the counterpart of H^{475} of ZntA, although the mutated WD protein was inactive and could not be phosphorylated by ATP [35]. The latter observation is consistent with the view that this histidine has catalytic functions other than a role as a constituent of the ATP-binding site.

In summary, we have used a bacterial Zn^{2+}-transporting P-type ATPase to study the roles of several residues, whose counterparts are mutated in the WD protein. Both characterization of the mutant ATPases and molecular modelling of the nucleotide-binding domain of the bacterial enzyme suggest that the residues Glu^{470}, His^{475}, Gly^{503} and Gly^{505} are likely to be involved in forming the binding site for ATP.

We thank Teija Inkinen and Katja Sissi for expert help with the laboratory work, Kimmo Mattila for help with Insight II and Mirkka Koivusalo for helping with the graphs. We thank the reviewers for a useful suggestion. Financial support was provided by the University of Helsinki, the Academy of Finland, the Magnus Ehrnrooth Foundation and the Sigrid Juselius Foundation.

REFERENCES

1 Toyoshima, C., Nakasako, Nomura, H. and Ogawa, H. (2000) Crystal structure of the calcium pump of sarcoplasmic reticulum at 2.6 Å resolution. Nature (London) **405**, 647–655
2 Toyoshima, C. and Nomura, H. (2002) Structural changes in the calcium pump accompanying the dissociation of calcium. Nature (London) **418**, 605–611
3 Abu-Abed, M., Mal, T. K., Kainosho, M., MacLennan, D. H. and Ikura, M. (2002) Characterization of the ATP-binding domain of the sarco(endo)plasmic reticulum Ca^{2+}-ATPase: probing nucleotide binding by multidimensional NMR. Biochemistry **41**, 1156–1164
4 Clausen, J. D., McIntosh, D. B., Vilsen, B., Woolley, D. G. and Andersen, J. P. (2003) Importance of conserved N domain residues Thr^{441}, Glu^{442}, Lys^{515}, Arg^{560}, and Leu^{562} of sarcoplasmic reticulum Ca^{2+}-ATPase for MgATP binding and subsequent catalytic steps: plasticity of the nucleotide binding site. J. Biol. Chem. **278**, 20245–20258
5 Jacobsen, M. D., Pedersen, P. A. and Jørgensen, P. L. (2002) Importance of Na,K-ATPase residue $\alpha 1\text{-}Arg^{544}$ in the segment Arg^{544}–Asp^{567} for high-affinity binding of ATP, ADP, or MgATP. Biochemistry **41**, 1451–1456
6 Patchornik, G., Munson, K., Goldshleger, R., Shainskaya, A., Sachs, G. and Karlish, S. J. D. (2002) The ATP-Mg^{2+} binding site and cytoplasmic domain interactions of Na^+,K^+-ATPase investigated with Fe^{2+}-catalyzed oxidative cleavage and molecular modeling. Biochemistry **41**, 11740–11749
7 Kubala, M., Hofbauerova, K., Ettrich, R., Kopecky, V., Krumscheid, R., Plašek, J., Teisinger, J., Schoner, W. and Amler, E. (2002) Phe^{475} and Glu^{446} but not Ser^{445} participate in ATP-binding to the α-subunit of Na^+/K^+-ATPase. Biochem. Biophys. Res. Comm. **297**, 154–159
8 McIntosh, D. B., Woolley, D. G., Vilsen, B. and Andersen, J. P. (1996) Mutagenesis of segment $^{487}Phe\text{-}Ser\text{-}Arg\text{-}Asp\text{-}Arg\text{-}Lys^{492}$ of sarcoplasmic reticulum Ca^{2+}-ATPase produces pumps defective in ATP binding. J. Biol. Chem. **271**, 25778–25789
9 Mitchinson, C., Wilderspin, A. F., Trinnaman, B. J. and Green, N. M. (1982) Identification of a labelled peptide after stoichiometric reaction of fluorescein isothiocyanate with the Ca^{2+}-dependent adenosine triphosphate of sarcoplasmic reticulum. FEBS Lett. **146**, 87–92
10 Hua, S., Inesi, G., Nomura, H. and Toyoshima, C. (2002) Fe^{2+}-catalyzed oxidation and cleavage of sarcoplasmic reticulum ATPase reveals Mg^{2+} and Mg^{2+}-ATP sites. Biochemistry **41**, 11405–11410
11 Gatti, D., Mitra, B. and Rosen, B. (2000) *Escherichia coli* soft metal ion-translocating ATPases. J. Biol. Chem. **275**, 34009–34012
12 Finney, L. A. and O'Halloran, T. V. (2003) Transition metal speciation in the cell: insights from the chemistry of metal ion receptors. Science (Washington, D.C.) **300**, 931–936
13 Loudianos, G. and Gitlin, J. D. (2000) Wilson's disease. Semin. Liver Dis. **29**, 353–364
14 Beard, S. J., Hashim, R., Membrillo-Hernandez, J., Hughes, M. N. and Poole, R. K. (1997) Zinc(II) tolerance in *Escherichia coli* K-12: evidence that the zntA gene (o732) encodes a cation transport ATPase. Mol. Microbiol. **25**, 883–891
15 Rensing, C., Mitra, B. and Rosen, B. P. (1997) The zntA gene of *Escherichia coli* encodes a Zn(II)-translocating P-type ATPase. Proc. Natl. Acad. Sci. U.S.A. **94**, 14326–14331
16 Okkeri, J. and Haltia, T. (1999) Expression and mutagenesis of ZntA, a zinc-transporting P-type ATPase from *Escherichia coli*. Biochemistry **38**, 14109–14116
17 Okkeri, J., Bencomo, E., Pietilä, M. and Haltia, T. (2002) Introducing Wilson disease mutations into the zinc-transporting P-type ATPase of *Escherichia coli*. The mutation P634L in the 'hinge' motif (GDGXNDXP) perturbs the formation of the E_2P. Eur. J. Biochem. **269**, 1579–1586
18 Bossemeyer, D. (1994) The glycine-rich sequence of protein kinases: a multifunctional element. Trends Biochem. Sci. **19**, 201–205
19 Grant, B. D., Hemmer, W., Tsigelny, I., Adams, J. A. and Taylor, S. S. (1998) Kinetic analyses of mutations in the glycine-rich loop of cAMP-dependent protein kinase. Biochemistry **37**, 7708–7715
20 Okkeri, J. and Haltia, T. (2002) Introducing Wilson disease mutations into the N domain of the Zn^{2+}-transporting P-type ATPase of *E. coli*: a glycine motif might be involved in binding of ATP. Abstracts of the 3rd International Meeting on Copper Homeostasis and Its Disorders: Molecular and Cellular Aspects, p. 79, 4–8 October (2002), Ischia, Italy
21 Thompson, J. D., Gibson, T. J., Plewniak, F., Jeanmougin, F. and Higgins, D. G. (1997) The CLUSTAL_X windows interface: flexible strategies for multiple sequence alignment aided by quality analysis tools. Nucleic Acids Res. **24**, 4876–4882
22 Rost, B. (1996) PHD: predicting one-dimensional protein structure by profile based neural networks. Methods Enzymol. **266**, 525–539
23 Fan, B. and Rosen, B. P. (2002) Biochemical characterization of CopA, the *Escherichia coli* Cu(I)-translocating P-type ATPase. J. Biol. Chem. **277**, 46987–46992
24 Hou, Z. and Mitra, B. (2003) The metal specificity and selectivity of ZntA from *Escherichia coli* using the acylphosphate intermediate. J. Biol. Chem. **278**, 28455–28461
25 Teramachi, S., Imagawa, T., Kaya, S. and Taniguchi, K. (2002) Replacement of several single amino acid side chains exposed to the inside of the ATP-binding pocket induces different extents of affinity change in the high and low affinity ATP-binding sites of rat Na/K-ATPase. J. Biol. Chem. **277**, 37394–37400
26 Glynn, I. M. (1985) The Na^+,K^+-transporting adenosine triphosphatase. In The Enzymes of Biological Membranes (Martonosi, A., ed.), pp. 35–114, Plenum Publishing Corp., New York
27 Møller, J. V., Juul, B. and Maire, M. (1996) Structural organization, ion transport and energy transduction of P-type ATPases. Biochim. Biophys. Acta **1286**, 1–51
28 McIntosh, D. B. (1998) The ATP binding sites of P-type ion transport ATPases: properties, structure, conformations, and mechanism of energy coupling. Adv. Mol. Cell. Biol. **23A**, 33–99
29 Solioz, M. and Vulpe, C. (1996) CPx-type ATPases: a class of P-type ATPases that pump heavy metals. Trends Biochem. Sci. **21**, 237–241
30 Lutsenko, S. and Kaplan, J. H. (1995) Organization of P-type ATPases: significance of structural diversity. Biochemistry **34**, 15607–15613
31 Zheng, J., Knighton, D. R., Ten Eyck, L. F., Karlsson, R., Xuong N., Taylor, S. S. and Sowadski, J. M. (1993) Crystal structure of the catalytic subunit of cAMP-dependent protein kinase complexed with MgATP and peptide inhibitor. Biochemistry **32**, 2154–2161
32 Reference deleted

33 Vetter, I. R. and Wittinghofer, A. (1999) Nucleoside triphosphate-binding proteins: different scaffolds to achieve phosphoryl transfer. Quart. Rev. Biophys. **32**, 1–56
34 Saraste, M., Sibbald, P. R. and Wittinghofer, A. (1990) The P-loop – A common motif in ATP- and GTP-binding proteins. Trends Biochem. Sci. **15**, 430–434
35 Tsivkovskii, R., Efremov, R. G. and Lutsenko, S. (2003) The role of the invariant His-1069 in folding and function of the Wilson's disease protein, the human copper-transporting ATPase ATP7B. J. Biol. Chem. **278**, 13302–13308
36 Petris, M. J., Voskoboinik, I., Cater, M., Smith, K., Kim, B.-E., Llanos, R. M., Strausak, D., Camakaris, J. and Mercer, J. F. B. (2002) Copper-regulated trafficking of the Menkes disease copper ATPase is associated with formation of a phosphorylated catalytic intermediate J. Biol. Chem. **277**, 46736–46742

Received 20 May 2003/5 September 2003; accepted 26 September 2003
Published as BJ Immediate Publication 26 September 2003, DOI 10.1042/BJ20030740

37 Danko, S., Yamasaki, K., Daiho, T., Suzuki, H. and Toyoshima, C. (2001) Organization of cytoplasmic domains of sarcoplasmic reticulum Ca^{2+}-ATPase in E_1-P and E_1-ATP states: a limited proteolysis study. FEBS Lett. **505**, 129–135
38 Kühlbrandt, W., Zeelen, J. and Dietrich, J. (2002) Structure, mechanism, and regulation of the *Neurospora* plasma membrane H^+-ATPase. Science (Washington, D.C.) **297**, 1692–1696
39 Xu, C., Rice, W. J., He, W. and Stokes, D. L. (2002) A structural model for the catalytic cycle of the Ca^{2+}-ATPase. J. Mol. Biol. **316**, 201–211
40 Voskoboinik, I., Mar, J. and Camakaris, J. (2003) Mutational analysis of the Menkes copper P-type ATPase (ATP7A). Biochem. Biophys. Res. Comm. **301**, 488–494